Detection of Specularity Using Color and Multiple Views *

Sang Wook Lee and Ruzena Bajcsy

GRASP Laboratory
Department of Computer and Information Science, University of Pennsylvania
3401 Walnut St., Philadelphia, PA 19082, USA

Abstract. This paper presents a model and an algorithm for the detection of specularities from Lambertian reflections using multiple color images from different viewing directions. The algorithm, called spectral differencing, is based on the *Lambertian consistency* that color image irradiance from Lambertian reflection at an object surface does not change depending on viewing directions, but color image irradiance from specular reflection or from a mixture of Lambertian and specular reflections does change. The spectral differencing is a pixelwise parallel algorithm, and it detects specularities by color differences between a small number of images without using any feature correspondence or image segmentation. Applicable objects include uniformly or nonuniformly colored dielectrics and metals, under extended and multiply colored scene illumination. Experimental results agree with the model, and the algorithm performs well within the limitations discussed.

1 Introduction

Recently there has been a growing interest in the visual measurement of surface reflectance properties in both basic and applied computer vision research. Most vision algorithms are based on the assumption that visually observable surfaces consist only of Lambertian reflection. Specularity is one of the major hindrances to vision tasks such as image segmentation, object recognition and shape or structure determination. Without any means of correctly identifying reflectance types, image segmentation algorithms can be easily misled into interpreting specular highlights as separate regions or as different objects with high albedo. Algorithms such as shape from shading and structure from stereo or motion can also produce false surface orientation or depth from the non-Lambertian nature of specularity. Therefore it is desirable to have algorithms for estimating reflectance properties as a very early stage or an integral part of many visual processes. In many industrial applications, there is a great demand for visual inspection of surface reflectance which is directly related to the quality of surface finish and paint.

Although the measurement of surface reflectance properties in applied physics has been the topic of many research efforts, only a few attempts in computer vision have been made until recently. There has been an approach to the detection of specularity with a single gray-level image using the Lambertian constraints by Brelstaff and Blake [BB88]. They attempted to extract maximal information from a single gray-scale image.

* This work was partly supported by E. I. du Pont de Nemours and Company, Inc. and partly by the following grants: Navy Grant N0014-88-K-0630, AFOSR Grants 88-0244, AFOSR 88-0296; Army/DAAL 03-89-C-0031PRI; NSF Grants CISE/CDA 88-22719, IRI 89-06770, and ASC 91 0813. We thank Ales Leonardis at University of Ljubljana, Slovenija, for his collaboration on our color research during his stay at the GRASP Lab. Special thanks to Steve Shafer at Carnegie Mellon University for helpful discussions and comments.

Although moderate success was demonstrated in detecting some apparent specularities, the problem is physically underconstrained.

In order to overcome the inherent limitations of a lack of information in a single image, the natural development is of course to collect more images in physically sensible ways, using optical and physical models which describe how surfaces appear according to the reflectance properties and sensor characteristics. Recently the computer vision field has increasingly incorporated methodologies derived from physical principles of image formation and sensing. There have been three types of approaches so far in solving the problem: collection of more images (1) with different light directions, (2) with different sensor polarization and (3) with different spectral sensors.

The photometric-stereo-type approaches are the most comprehensive methods in investigating surface reflectance properties. The objective of the approaches is to obtain object shape and both Lambertian and specular reflectances separately, and more than two light sources are required for recently proposed algorithms [NIK90] [Td91]. The basic technique of the photometric-stereo-type approaches is the switching of illumination sources. The direction and the degree of the collimation of the illumination need to be strictly controlled. Therefore, application is restricted to *dark-room* environments where the illumination can be strictly controlled.

Wolff proposed a method of detecting specularities using the analysis of the polarization of reflected light [Wol89]. The polarization approach places restrictions on illumination directions with only two polarizer angles. Although many angles of polarizer filters are suggested for extended light, it is yet to be demonstrated extensively how the algorithm performs for rough surfaces under extended light sources.

The dichromatic model [Sha85] proposed by Shafer has been the key model to the recent specularity detection algorithms using color, such as the ones by Klinker, Shafer and Kanade, by Gershon, by Healey and Binford, and more recently by Bajcsy, Lee and Leonardis [KSK88] [Ger87] [HB89] [BLL90]. The basic limitation of the color algorithms is that objects have to be only colored dielectrics to use the dichromatic model. Another limitation is the requirement for image segmentation as an essential part of the algorithm. For image segmentation, it is usually assumed that object surface reflectance is spatially piecewise uniform and scene illumination is singly colored. The algorithms using color detect only probable specularities, since variation in object reflectances or in illumination color can result in the spectral variation of the scene that may be interpreted as the presence of specularities.

All the algorithms mentioned above have their limitations as well as advantages. The assumptions involved with each algorithm pose limitations on the applicable domains of the objects and illumination. The primary objective of the research presented in this paper was to develop a model applicable to more general object and illumination domains than the ones of previous algorithms, using color and multiple views. As mentioned above the photometric-stereo-type approaches require strict control of illumination light, and the polarization method has a restriction in illumination directions. Illumination control is not possible in general environments. Examples include outdoor inspection, and indoor or outdoor navigation or exploratory environments. Even for indoor inspection, a well controlled dark room is not always available.

The color segmentation approaches impose restrictions on the object and illumination color, because of the limited information in a single color image. Therefore it would be desirable to have any extra information in order to overcome the limitations in the object and illumination domains. The idea of moving the observer is motivated by the concept of active observer [Baj88]. It is well accepted that with extra views added, extra geometric

information can be obtained. For low-level vision problems of shape or structure, it has been demonstrated that many ill-posed problems become well-posed if more information is collected by active sensors [AB87]. Although the paradigms for shape or structure based on feature correspondence cannot be directly applied to the study of reflectance properties, the idea of an active observer motivates the investigation of new principles by physical modeling in obtaining more information. A question to be answered is what kind of extra spectral information can be obtained by a moving camera without considering object geometry. If there is any, it may alleviate the limiting assumptions required for color segmentation approaches and provide higher confidence in detecting specularities.

In this paper, a model is presented for explaining extra spectral information from two or more views, and a specularity detection algorithm, called spectral differencing, is proposed. The algorithm does not require any assistance from image segmentation since it does not rely on the dichromatic model. The algorithm only exploits the variation of different spectral composition of reflection depending on viewing directions, therefore it does not require any geometric manipulation using feature correspondence. An important principle used is the the *Lambertian consistency* that the Lambertian reflection does not change its brightness and spectral content depending on viewing directions, but the specular reflection or the mixture of Lambertian and specular reflections can change.

Basic spectral models for reflection mechanisms are introduced in Sect. 2, and Sect. 3 explains how the measured color appears in a three-dimensional color space. A model is also established in Section 3 for explaining the spectral difference between different views for uniform dielectrics under singly colored illumination. The detection algorithm of spectral differencing is also described in Sect. 4, and Sect. 5 discusses the spectral differencing for various objects that include nonuniformly colored dielectrics and metals, under multiply colored illumination. Experimental results are presented in Sect. 6.

2 Reflection Model

Physical models for light-surface interaction and for sensing are crucial in developing the algorithms for detection of specularity. Several computer vision researchers have introduced useful models based on the physical process of image-forming [TS67] [BS63] [Sha85] [LBS90] [HB89]. Although there are certain approximations, the models introduced in this section are generally well accepted in computer vision for their good approximation of the physical phenomena.

2.1 Reflection Type

There are two physically different types of reflections for dielectric materials according to the dichromatic model proposed by Shafer [Sha85], interface or surface reflection and body or sub-surface reflection. Reflection types are summarized in Fig. 1. The surface or interface reflection occurs at the interface of air and object surface. When light reaches an interface between two different media, some portion of the light is reflected at the boundary, resulting in the interface reflection, and some refracted into the material. The ratio of the reflected to the refracted light is determined by the angle of incidence and the refractive indices of the media. Since the refractive indices of dielectric material are nearly independent of wavelength (λ) over the visible range of light (400 nm to 700 nm of wavelength), interface reflectance of dielectrics can be well approximated as flat spectrum as shown in Fig. 1 [LBS90].

The refracted light going into a sub-surface is scattered from the internal pigments and some of the scattered light is re-emitted randomly resulting in the body or sub-surface reflection. Thus the reflected light has the Lambertian property due to the randomness of the re-emitted light direction. The Lambertian reflection means that the amount of reflected light does not depend on the viewing direction, but only on the incident light. Depending on the pigment material and distribution, the reflected light undergoes a spectral change, i.e., the spectral power distribution (SPD) of the reflected light is the product of the SPD of the illumination and the body reflectance. The fact that the interface and the body reflections are often spectrally different is the key concept of the dichromatic model, and central to many detection algorithms by color image segmentation.

For metals, electromagnetic waves cannot penetrate into the material by more than skin depth because of the large conductance that results in large refactive index. Therefore all the reflections occur at the interface, and due to the lack of the body reflection, metals are unichromatic [HB89]. Interface reflections from most metals are white or grey, e.g., from silver, iron, aluminum. However, there are reddish metals such as gold and copper.

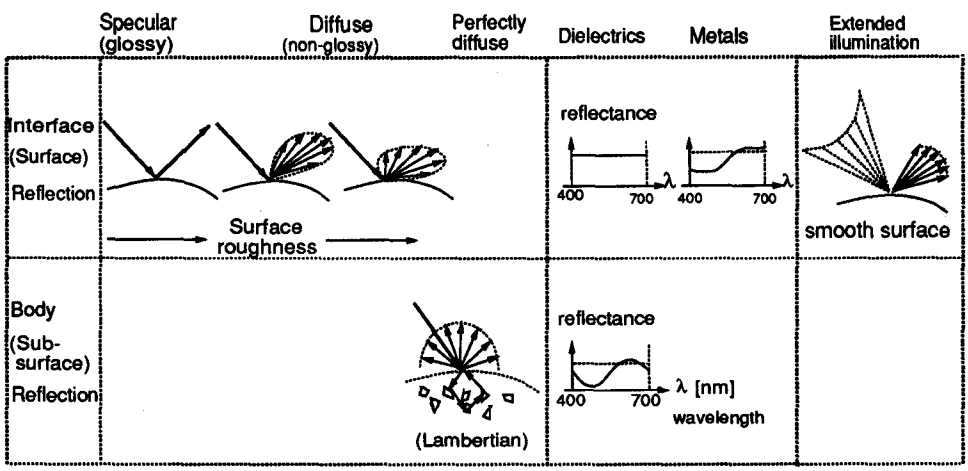

Fig. 1. Reflection models

Reflections can also be categorized as glossy specular and nonglossy diffuse reflections depending on the appearance. This categorization depends on the degree of diffusion in the reflected light direction. Body reflection can be modeled as a perfectly diffuse reflection, i.e., Lambertian reflection. Specularity results from interface reflection, and the reflected direction of the specularity depends both on the illumination direction and surface orientation. The specularity is diffused depending on the surface roughness. There have been some models that describe the scattering of light by rough surfaces. The physical modeling of Beckman and Spizzichino [BS63] is based on the electromagnetic scattering of light waves at rough surfaces. The simpler geometric modeling by Torrance and Sparrow is widely accepted in computer vision and graphics as a good approximation of the physical phenomenon [TS67]. The Torrance-Sparrow model assumes that a surface is composed of small, randomly oriented, mirror-like microfacets, and the Gaussian function is used for the distribution of the microfacets. A rougher surface has a wider

distribution of the microfacets, and the direction of the reflected light is more diffuse, as is illustrated in Fig. 1.

Diffusion in the direction of the interface reflection may result from extended and diffuse illumination as shown in Fig. 1. When illumination is extended and diffuse, the incident angle of light to a surface patch is extended and interface reflections at even a smooth surface appear diffusely. When the surface is rough, the reflection is more diffuse.

In this paper, "specular reflection" is used to denote interface reflection, while "Lambertian reflection" is used to denote body reflection. Use of "surface reflection" for denoting the interface reflection is avoided, since, in a wider sense, it means all the reflections from surface and sub-surface. In this paper, "surface reflection" is used in the wider sense. When "diffuse reflection" is used, it can be either diffuse interface or body reflection.

2.2 Representation and Sensing

For singly colored illumination $e(\lambda)$, whether geometrically collimated or extended, scene radiance is given as the product of illumination and reflection, i.e.,

$$L_r(\lambda) = e(\lambda)s(\lambda). \tag{1}$$

where $s(\lambda)$ is the reflection, and λ is the wavelength of light. The surface reflection is the linear combination of specular and Lambertian reflections with the different geometric weighting factors, i.e.,

$$s(\lambda) = \rho_S(\lambda)G_S(\theta_r, \phi_r) + \rho_B(\lambda)G_B \tag{2}$$

where $\rho_S(\lambda)$ and $\rho_B(\lambda)$ are the specular and the Lambertian reflectances, i.e., Fresnel reflectance and albedo, respectively, (θ_r, ϕ_r) denotes the reflection direction, and $G_S(\theta_r, \phi_r)$ and G_B are the purely geometric factors which are independent of spectral information. The geometric factors are determined by illumination and viewing directions with respect to surface orientation. Observation of the specular reflection is highly dependent both on the viewer and on the illumination directions, while observation of body reflection depends only on the illumination direction.

Note that, for metals, $\rho_B(\lambda)G_B$ is 0, and for dielectrics, G_B is independent of the viewing angle (θ_r, ϕ_r). It has been reported that the spectral composition of Lambertian reflection slightly changes when the incident light direction approaches 90° with respect to surface normal (glancing incidence) [HB89]. However this effect is small even near the glancing incidence of light, and thus is neglected in the model.

When there are more than one illumination sources with different colors from different directions, the addition of reflections under different illumination sources

$$L_r(\lambda) = e_1(\lambda)s_1(\lambda) + e_2(\lambda)s_2(\lambda) + .. \tag{3}$$

is used for establishing models presented in this paper.

The color image sensing is usually performed with a CCD camera using filters of different spectral responses. With 3 filters (usually R, G and B), the quantum catch or the measured signal from the camera is given by

$$q_k = \int_{\lambda_1}^{\lambda_2} L_r(\lambda)Q_k(\lambda)d\lambda, \tag{4}$$

where $Q_k(\lambda)$ and q_k for $k = 0, 1, 2$ are the spectral response of the $k-$th filter, and the camera output through the $k-$th filter, respectively. The wavelengths $\lambda_1 = 400\ nm$ and $\lambda_2 = 700\ nm$ cover the range of the visible spectrum.

In many works in color science, interpretation of measured color is often performed with three-dimensional color space on three basis functions, as well as the RGB sensor space, and some basis functions have been suggested and used [Coh64] [MW86]. In this paper, the scene radiance model is explained in a general three-dimensional color space although the proposed algorithm is implemented with the RGB space.

The scene radiance $L_r(\lambda)$ can be approximated with three basis functions $S_0(\lambda)$ $S_1(\lambda)$ and $S_2(\lambda)$ as

$$L_r(\lambda) = \sum_{i=0}^{2} \gamma_i S_i(\lambda), \tag{5}$$

where γ_i's are the scalar weighting factors. The relationship between the sensor responses q_k's and γ_i's is a linear transformation given as

$$\underline{q} = \underline{\Lambda}\ \underline{\gamma}, \quad \underline{\gamma} = \underline{\mathbf{V}}\ \underline{q}, \quad \Lambda_{ki} = \int_{\lambda_1}^{\lambda_2} S_i(\lambda) Q_k(\lambda) d\lambda, \tag{6}$$

where $\underline{q} = [q_0, q_1, q_2]^T$, $\underline{\gamma} = [\gamma_0, \gamma_1, \gamma_2]^T$, $\underline{\mathbf{V}} = \underline{\Lambda}^{-1}$, and Λ_{ki} is the element of $\underline{\Lambda}$ in the k-th row and i-th column.

3 Spectral Scene Radiance from Different Views

The vetor $\underline{q}$ or the linear transformation $\underline{\gamma}$ represents the measured scene radiance that results from the illumination and reflectance color and from geometric weighting. In this section, it is explained how the measured $\underline{q}$'s or $\underline{\gamma}$'s from a color image appear in a general three-dimensional color space, and a model is established for a specularity detection algorithm using color information from different views. The three-dimensional spectral space constructed from the RGB values or from the basis functions $S_0(\lambda)$ $S_1(\lambda)$ and $S_2(\lambda)$ is generally called **S** space in this paper.

In this section, the spectral scene radiance is considered only for dielectric objects with uniform reflectance under singly colored illumination. Dielectric materials with reflectance variation and metals under multiply colored illumination will be discussed in Sect. 5.

3.1 Lambertian Reflection

For Lambertian surfaces, shading results from the variation in surface orientations relative to illumination directions. In the **S** space, the scene radiance generated by shaded Lambertian reflections form linear clusters.

Scene radiance from Lambertian reflection is given from (1), (2) and (5) by

$$L_r(\lambda) = e(\lambda)\rho_B(\lambda)G_B = \sum_{i=0}^{2} \gamma_i S_i(\lambda). \tag{7}$$

Shading on a surface of uniform reflectance is due to variations in geometry G_B in (7), and the spectral curve of $L_r(\lambda)$ is scaled depending on G_B. When the spectral curves of $e(\lambda)$ and $\rho_B(\lambda)$ are assumed to be constant over the differently shaded object patches, the ratio of γ_i's such as γ_1/γ_0 and γ_2/γ_0 are independent of shading by G_B, and thus the ratios of γ_i's are constant over the differently shaded patches. Therefore γ_i's form a linear cluster in the S space as shown Fig. 2 (a). This property has been previously suggested

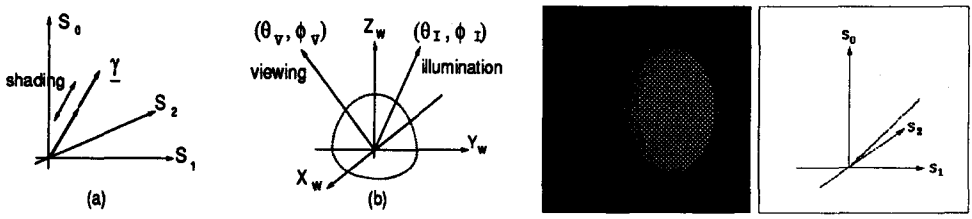

Fig. 2. Shading; (a) linear cluster (b) coordinates for simulated images (c) Lambertian shading (d) linear cluster in S space

and used in segmentation [Sha85] [KSK88]. The orientation of the vector $\underline{\gamma}$ is determined by the Lambertian reflectance and illumination, and independent of geometry.

Examples are shown by simulation with a spherical object for the geometry shown in Fig. 2 (b). Figure 2 (c) and (d) show a simulated image of a sphere, and its color cluster in the **S** space with $(\theta_V, \phi_V) = (35^o, 0^o)$ and $(\theta_I, \phi_I) = (0^o, 0^o)$, respectively. For the simulation, a spectrum measured from a real blue color plate is used for the reflectance, and a linear cluster is shown in the **S** space for spectrally flat neutral light. The Fourier basis functions $S_0(\lambda) = 1$, $S_1(\lambda) = sin\lambda$ and $S_2(\lambda) = cos\lambda$ are used for the **S** space in Fig. 2 (d).

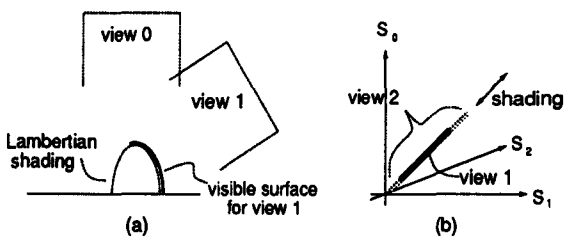

Fig. 3. Lambertian surface from multiple views (a) geometric illustration (b) color clusters in S space

Figure 3 (a) illustrates Lambertian surfaces at two different views. When illumination is the same between different views, Lambertian reflections from a surface appear in the same locations in the **S** space regardless of the viewing angle. However occlusion of surfaces by other object surfaces can affect the distribution of color points in the linear cluster. For the view 1, not all the Lambertian surfaces are visible due to occlusion, and color clusters from only a part of the object are observable in the **S** space. The visible color clusters are shown as a dark solid line in Fig. 3 (b). On the other hand, those invisible surfaces are disoccluded in the view 0. Disocclusion is the emergence of object points or patches into visibility from behind occlusion. Depending on the shading of the disoccluded part, emerging color clusters of the object from occlusions can be included in the linear cluster, or can appear outside the cluster yet in the extended line, since the disoccluded part is a part of the same object. An example of spectral difference between the two views is shown as the gray lines in Fig. 3 (b). Note that orthographic projections are illustrated in Fig. 3 (a), but the above explanation also applies to perspective projections.

3.2 Specular Reflection

Highlights are due to specular reflections from dielectrics or metals. Since scene radiance from specular reflection is given by

$$L_r(\lambda) = e(\lambda)\rho_S(\lambda)G_S(\theta_r, \phi_r) = \sum_{i=0}^{2} \gamma_i S_i(\lambda). \quad (8)$$

Specular reflections alone, e.g., from metals or from black dielectrics, form linear clusters in the **S** space like the Lambertian reflections. Because of the neutral reflectance, the direction of the linear cluster from the dielectrics is the same as the illumination direction in the **S** space. On the other hand, the direction of a linear cluster from a metal is determined by the spectral reflectances and illumination.

For dielectrics, specular reflections are added to Lambertian reflections as shown in Fig. 4 (a). With extended illumination or with roughened surfaces, the distribution of specular reflections can spatially vary over a wide area of the shaded surface as shown in Fig. 4 (a). Therefore specular reflections form planar clusters which include the linear clusters formed by shading on the **S** space. The orientation of the plane is dependent on the illumination color. When illumination is well collimated and the surface is smooth the color clusters form generally skewed T or L shapes as suggested by Shafer [Sha85], since the specular reflection is distributed in a small range of shading and forms a linear cluster connected to a linear cluster of the Lambertian reflections. However, when illumination is spatially extended or the surface is rough, the color clusters generally form skewed P shapes, and the color cluster of specular reflections is planar and coplanar with a linear cluster of Lambertian reflections.

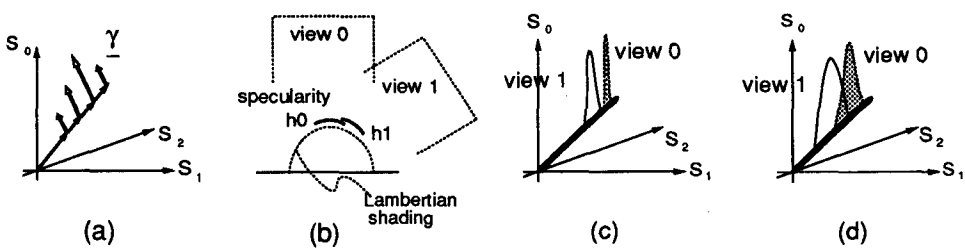

Fig. 4. Specularity; (a) in S space (a) geometric illustration for multiple views (b) color clusters in S space for smooth surface (c) for rough surface

Figure 4 (b) illustrates positions of specularities on shaded a Lambertian surface at two different views. Depending on the viewing directions, the specularities h0 and h1 in Fig. 4 (b) are located on spatially different shaded surfaces.

In the **S** space, color clusters from the specularities are located on differently shaded Lambertian clusters as shown in Fig. 4 (c) and (d). The shape and position of the specular clusters depend on viewing directions and surface roughness as well as on surface orientations and illumination directions. Figures 5, 6 and 7 show the color clusters of specular and Lambertian reflections by simulation for different surface roughness and for different collimation of neutral illumination. As shown in the figures, the planar color clusters in the **S** space are differently shaped depending on the viewing directions.

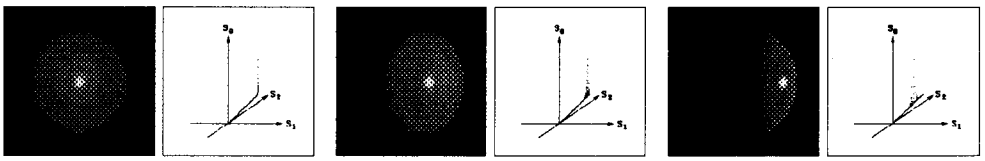

Fig. 5. Reflection for smooth surface and collimated illumination for $(\theta_I, \phi_I) = (0°, 0°)$ $(\theta_V, \phi_V) = (0°, 0°)$, $(35°, 0°)$, $(70°, 0°)$ and relative surface roughness = 0.1

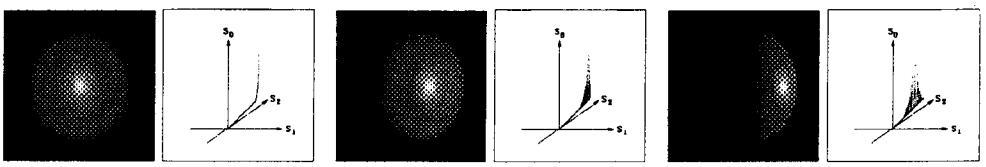

Fig. 6. Reflections for smooth surface and extended illumination for $0° < \theta_I < 30°$, $0° < \phi_I < 360°$, $(\theta_V, \phi_V) = (0°, 0°)$, $(35°, 0°)$, $(70°, 0°)$ and relative surface roughness = 0.1

Except for Lambertian occlusions, the spectral difference between the views results from specularities, although it does not account for all the specularities due to the overlap of specularities in the **S** space. In Fig. 4 (c), all the specularities are the spectral difference, but in Fig. 4 (d), only part of the specularities is the spectral difference since there is an overlap between the specular clusters from the two views. Since the amount of spectral displacement of the specularities is determined by the difference in the viewing angles, object shape, variations in object shape and illumination distribution, it is difficult to predict it in a simple manner for general objects and illumination. However the general rule is that as the difference in the viewing directions increases, the spectral overlaps between the specularities decrease. If the object shape varies more geometrically, specularities are likely to change more. Specularities often completely disappear depending on the views.

A point to note is occlusion by specularity. In some views, specularities can be distributed such that some Lambertian shading may not be visible at all. In other views, the Lambertian shading may appear as new clusters in the **S** space, therefore can be detected as spectral difference.

4 Spectral Differencing Algorithm

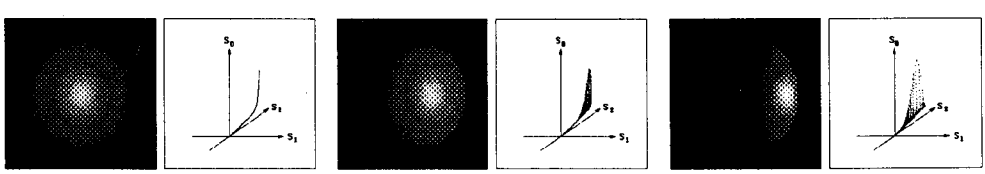

Fig. 7. Reflections for rough surface and collimated illumination for $(\theta_I, \phi_I) = (0°, 0°)$ $(\theta_V, \phi_V) = (0°, 0°)$, $(35°, 0°)$, $(70°, 0°)$ and relative surface roughness =0.3

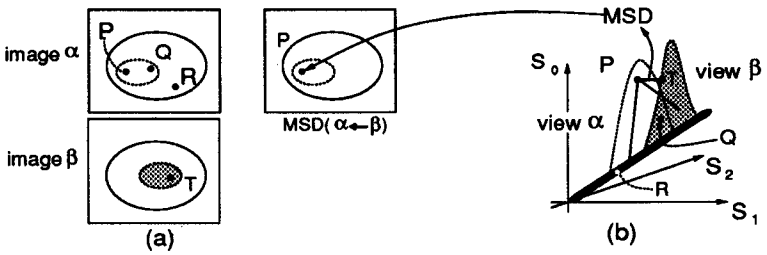

Fig. 8. Spectral differencing (a) images from different views (b) color clusters in S space

For two color images with different viewpoints, the spectral differencing is an algorithm for finding the color points of one image which do not overlap with any color points of the other image in a three-dimensional spectral space (e.g., the S space or a sensor space with RGB values). In order to detect the view-inconsistent color points, the spectral differencing algorithm computes the minimum spectral distance (MSD) images. The computation of an MSD image is explained as follows with an example shown in Fig. 8.

Let α and β be two color images obtained from two different views. The notation

$$\mathsf{MSD}(\alpha \leftarrow \beta)$$

represents the MSD image of α from β. A pixel value of the MSD image MSD($\alpha \leftarrow \beta$) is the minimum value of all the spectral distances between the pixel in the image α and all the pixels in the image β. The spectral distance is defined as the euclidean distance between two color points in a three-dimensional spectral space. Any MSD's above a threshold indicate the presense of specular reflections or Lambertian disocclusions. The threshold for the MSD image is determined only by sensor noise, and no adjustment is required for different environments.

Figure 8 (a) illustrates two images of an object with specularity from two different viewpoints, and the corresponding color clusters in the S space are shown in Fig. 8 (b). The pixel P in the image α is distantly located from the specular and Lambertian color points of the image β, which indicates specular reflection at P. On the other hand, the Lambertian reflections from the views α and β have the same linear cluster. Since the pixel R in the region of Lambertian reflection in the image α is close to the Lambertian points in the image β in the **S** space, it should not be detected by spectral differencing.

The spectral differencing does not detect all the specularities in a view. In Fig. 8 (b), the color point from the pixel Q is located in the overlapped region between the planar clusters in the views α and β. Since Q is located within the planar cluster formed by specular reflection in the view β, it is hard to detect Q as a specular reflection when the color points in planar cluster in the view β is densely populated. The specular reflection at Q can be detected by this algorithm only when the color points in the planar cluster in the view β are sparsely distributed around Q.

In this paper, no study for finding faster algorithms for spectral differencing is presented. However, an important point to note is that the algorithm is pixelwise parallel. Therefore with a parallel machine, the computation time depends only on the degree of achievable parallelism of the machine.

Spectral differencing is performed for the three simulated images shown in Fig. 7, and the three images and the MSD images are shown in Fig. 9. The table of image arrangement is also shown in Fig. 9. All the MSD images in Fig. 9 show detected specularities.

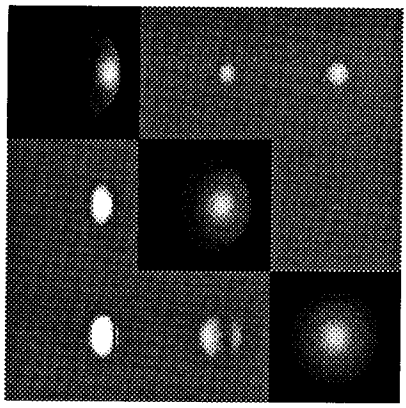

view 0	MSD(1←0)	MSD(2←0)
MSD(0←1)	view 1	MSD(2←1)
MSD(0←2)	MSD(1←2)	view 2

Fig. 9. Spectral differencing for the simulated images in Fig. 9

The detection is always an underestimation of the specular region except for disocclusions. The disoccluded Lambertian reflections are shown in MSD(0←2), and there is a region detected due to specular disocclusion in MSD(1←2). In the view 2, the brightest shading is occluded by specularities.

5 Extended Object and Illumination Domain

In the previous sections, the spectral differencing is explained only for dielectrics with uniform reflectance under singly colored illumination. In this section, it is discussed that the spectral differencing is effective as well for various objects under multiply colored illumination.

5.1 Dielectrics with Reflectance Variation

When the reflectance $\rho_B(\lambda)$ is not uniform in color for a surface, but has gradual variation, the measured colors from shaded Lambertian surface do not form a linear cluster. The color cluster is dispersed depending on the degree of variation in the reflectance, as illustrated in Fig. 10 (a). Some natural surfaces such as wood grains, leaves and human faces have variation in reflectance.

Figure 10 illustrates the color clusters of a dielectric object with varying Lambertian reflectance. The Lambertian cluster is not linear due to the variation in $\rho_B(\lambda)$ in (1) which is written again below

$$L_r(\lambda) = e(\lambda)[\rho_S(\lambda)G_S(\theta_r, \phi_r) + \rho_B(\lambda)G_B]. \tag{9}$$

Even with the volume or planar clusters from Lambertian reflection, the *Lambertian consistency* applies (except for disocclusion), since the geometric factor G_B is independent of the viewing angle (θ_r, ϕ_r). On the other hand, specularities are mixed with differently shaded and colored Lambertian reflections depending on the viewing directions, since the geometric factor $G_S(\theta_r, \phi_r)$ for specular reflections varies depending on (θ_r, ϕ_r) in (9). Therefore the spectral differencing can detect specularities that have different spectral values over different views.

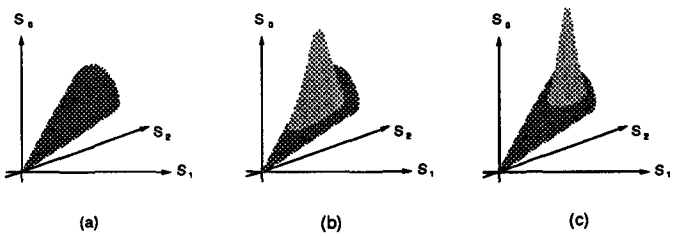

Fig. 10. Dielectric with variation in reflectance

5.2 Dielectrics under Multiply Colored Illumination

Under multiply colored illumination, Lambertian clusters even from uniform dielectrics are not linear, but dispersed in the S space due to the variation in the illumination. However, the distribution of Lambertian color points is invariant with respect to viewing directions except for occlusions and disocclusions. On the other hand, the distribution of color points from specularities changes depending on the viewing directions due to the different mixture of colors between the specular reflections or between the specular and Lambertian reflections.

From (1) and (3), scene radiance with two illumination sources is given as

$$\begin{aligned} L_r(\lambda) = {} & \rho_S(\lambda)[e_1(\lambda)G_{S1}(\theta_r, \phi_r) + e_2(\lambda)G_{S2}(\theta_r, \phi_r)] \\ & + \rho_B(\lambda)[e_1(\lambda)G_{B1} + e_2(\lambda)G_{B2}], \end{aligned} \tag{10}$$

and Fig. 11 shows an example with two illumination sources. The Lambertian reflection forms a planar cluster with two illumination colors, and independent of (θ_r, ϕ_r). When there are more than two illumination sources with different colors, or when $\rho_B(\lambda)$ varies, the Lambertian reflection generally forms a volume cluster.

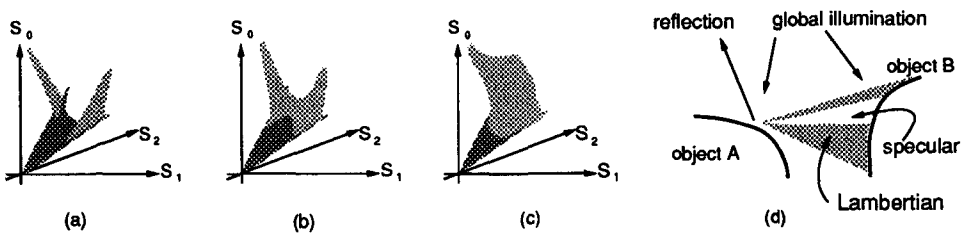

Fig. 11. (a) (b) (c) Dielectric under multiply colored illumination from varying viewpoints (d) inter-reflection

The specular reflection is a linear combination of the two components from the two illumination colors e_1 and e_2. Each component as well as the combination varies depending on the viewing angle (θ_r, ϕ_r). When the specularities appear in different Lambertian surfaces without overlap, they represent illumination colors in two directions separately as shown in Fig. 11 (a). When the viewing geometry changes, the specularities can be mixed in a surface and produces new specular points in the S space as shown in Fig. 11 (b) and

(c). Therefore spectral differences result from specular reflections except for Lambertian disocclusions.

Inter-reflection When there are many objects, the object surface of interest receives not only the light from the illumination sources, but the reflected light from the other objects. The latter causes a local change of illumination, as illustrated in Fig. 11 (d). The reflection from more-than-one surfaces is called inter-reflection. Object surfaces for the first reflection are secondary light sources which are generally extended depending on the object size. Together with the direction global illumination, the first reflection provides multiply colored illumination for other surfaces as shown in Fig. 11 (d), and influences the distribution of color clusters of the other surfaces. In indoor environments, reflections from walls and ceiling are the major sources of ambient light.

5.3 Metals

Since metals have only specular reflectance, there are no Lambertian reflections. When there is only a single illumination source for a uniform metallic object without any ambient light, only a linear cluster appears in the S space. In most cases, however, metals are observed with reflections from many light sources that include scene illumination sources and many surrounding objects. Especially shiny metals reflect all the incoming light from surrounding objects. The mixture of reflected light from direct illumination sources and inter-reflections changes depending on viewing directions, with different geometric weighting of the light coming from different directions. Therefore the color changes due to the different mixture of light can be detected by spectral differencing.

An example is shown in Fig. 12 for the scene radiance under two different illumination sources. Without any Lambertian components in (10), the scene radiance is a combination of two specular components as

$$L_r(\lambda) = \rho_S(\lambda)[e_1(\lambda)G_{S1}(\theta_r, \phi_r) + e_2(\lambda)G_{S2}(\theta_r, \phi_r)]. \tag{11}$$

When the two components separately appear in a measured image without being mixed, the color points in the S space form two different linear clusters as shown in (a). Depending on the viewing directions, the two colors can be differently combined as shown in (b) and (c), and the spectral differencing can detect different reflections in color.

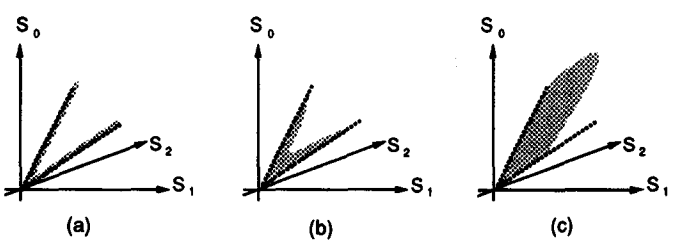

Fig. 12. Metal under multiply colored illumination from varying viewpoints

6 Experimental Results and Discussion

In order to test the algorithm, some experiments were carried out on various objects all under multiply colored illumination. Illumination was provided by fluorescent light in two directions on the ceiling of the room and by tungsten light in another direction located closer to the objects. Four large fluorescent light tubes were used, two in each direction, and half of a tungsten light bulb was screened with white paper for diffusing the light and the remaining half was exposed. White walls and ceiling provide some ambient illumination. The illumination environment is a normal indoor one, unlike a dark room with collimated light.

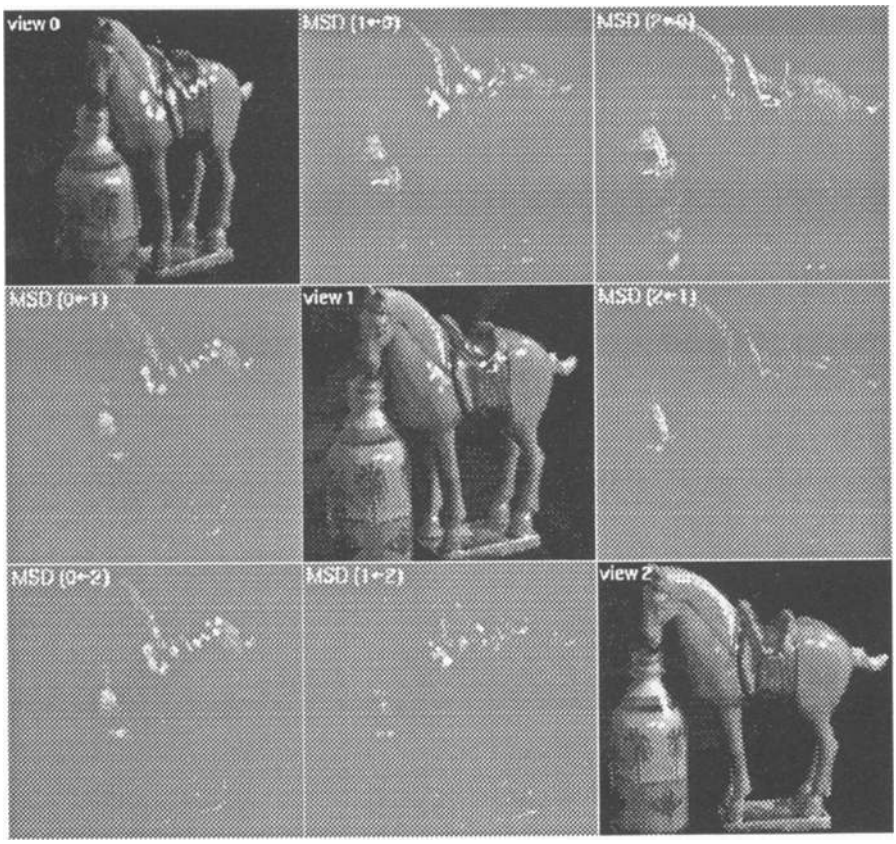

Fig. 13. Specularity with variation in Lambertian reflectance

Figure 13 shows images of dielectric objects with smooth reflectance variation. The arrangement of measured images and MSD images is the same as that in Fig. 9. The porcelain horse has variation in its Lambertian reflectance, especially near its shoulder and the saddle. The MSD images show nonzero values where most of the sharp and diffuse specularities are. The threshold for the MSD images was experimentally determined as 2 in terms of the RGB input values (0-255).

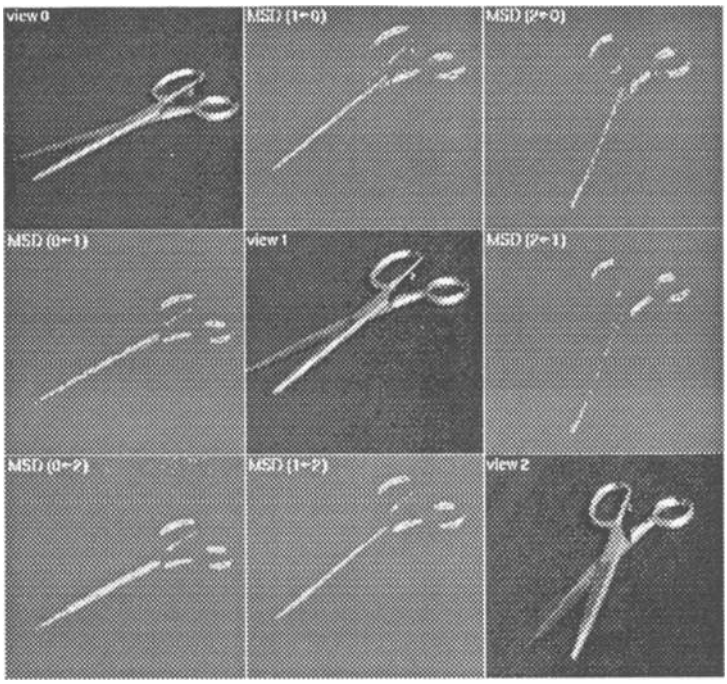

Fig. 14. Specularity from metal

Figures 14 shows the results from a metallic object. The MSD images clearly show most of the sharp specularities, indicating that the spectral movement of the sharp specularities are large. Some of the diffuse specularities are also detected. For a given shape of object, the diffuse specularities are better detected with wider angles between the views. In fact, all the reflections from metals are specular reflections. However the very diffuse reflections are not detectable when they form densely populated color clusters like Lambertian reflections in a three-dimensional color space, and the different viewing geometry does not generate enough spectral differences.

The experimental results with real objects demonstrate that spectral differencing is a remarkably simple and effective way of detecting specularities without any geometric reasoning. The algorithm does not require any geometric information or image segmentation. Therefore it can provide independent information to other algorithms such as structure from stereo, structure from motion, or image segmentation algorithms. Since the spectral differencing does not depend on any image segmentation, there are no assumptions of uniformly colored dielectric objects and singly colored illumination.

A limitation of the spectral differencing algorithm is that disocclusions are detected together with specularities and they are indistinguishable. Separation between the specularity and disocclusion may be achieved with other algorithms such as color image segmentation algorithms [BLL90]. As mentioned above, the spectral differencing algorithm can be easily intergrated with a color segmentation algorithm, and we are currently developing some integrated methods.

7 Conclusion

In this paper, an algorithm is proposed for the detection of specularities based on physical models of reflection mechanisms. The algorithm, called spectral differencing, is pixelwise parallel, and it detects specularities based on color differences between a small number of multiple color images without any geometric correspondence or image segmentation. The key contribution of the spectral differencing algorithm is to suggest the use of multiple views in understanding reflection properties. Although multiple views have been one of the major cues in computer vision in obtaining object shape or structure, it has not been used for obtaining reflection properties. The spectral differencing algorithm is based on the *Lambertian consistency*, and the object and illumination domains include nonuniformly colored dielectrics and metals, under multiply colored scene illumination. The experimental results conform well to our model based on the *Lambertian consistency*.

References

[AB87] J. Aloimonos and A. Badyopadhyay. Active vision. In *Proc. 1st Int. Conf. on Computer Vision*, pages 35–54, 1987.

[Baj88] R. Bajcsy. Active perception. *Proceedings of the IEEE*, 76:996–1005, 1988.

[BB88] G. Brelstaff and A. Blake. Detecting specular reflections using lambertain constraints. In *Proc. of IEEE Int. Conf. on Computer Vision*, pages 297–302, Tarpon Springs, FL, 1988.

[BLL90] R. Bajcsy, S.W. Lee, and A. Leonardis. Color image segmentation with detection of highlights and local illumination induced by inter-reflections. In *Proc. 10th International Conf. on Pattern Recognition*, Atlantic City, NJ, June 1990.

[BS63] P. Beckman and A. Spizzichino. *Scattering of Electromagnetic Waves from Rough Surfaces*. Pergamon Press, London, UK, 1963.

[Coh64] J. Cohen. Dependency of the spectral reflectance curves of the munsell color chips. *Psychon. Sci.*, 1:369–370, 1964.

[Ger87] R. Gershon. *The Use of Color in Computational Vision*. PhD thesis, Department of Computer Science, University of Toronto, 1987.

[HB89] G.H. Healey and T.O. Binford. Using color for geometry-insensitive segmentation. *Journal of the Optical Society of America*, 6, 1989.

[KSK88] G.J. Klinker, S.A. Shafer, and T. Kanade. Image segmentation and reflection analysis through color. In *Proceedings of the DARPA Image Understanding Workshop*, pages 838–853, Pittsburgh, PA, 1988.

[LBS90] H.-C. Lee, E. J. Breneman, and C. P. Schulte. Modeling light reflection of computer vision. *IEEE Trans. PAMI*, 12:402–409, 1990.

[MW86] L. T. Maloney and B. A. Wandell. A computational model of color constancy. *Journal of the Optical Society of America*, 1:29–33, 1986.

[NIK90] S. K. Nayar, K. Ikeuchi, and T. Kanade. Determining shape and reflectance of hybrid surfaces by photometric sampling. *IEEE Trans. Robo. Autom.*, 6:418–431, 1990.

[Sha85] S.A. Shafer. Using color to separate reflection components. *COLOR Research and Application*, 10:210–218, 1985.

[Td91] H.D. Tagare and R. J. deFigueiredo. Photometric stereo for diffuse non-lambertian surface. *IEEE Trans. PAMI*, 13:, 1991.

[TS67] K. E. Torrance and E. M. Sparrow. Theory for off-specular relfection from roughened surfaces. *Journal of the Optical Society of America*, 57:1105–1114, 1967.

[Wol89] L. B. Wolff. Using polarization to separate reflection components. In *Proc. of IEEE Conference on Computer Vision and Pattern Recognition*, pages 363–369, San Diago, CA, 1989.

This article was processed using the LaTeX macro package with ECCV92 style